Electronic supplementary information

Ce-regulating defect and morphology engineering for efficiently enhancing the piezocatalytic performances of BiOBr

Lihui Zhan,‡ Jindou Hu,‡ Yali Cao*, Xueer Ning, Jing Xie, Zhenjiang Lu and Aize Hao*

State Key Laboratory of Chemistry and Utilization of Carbon Based Energy Resources, College of Chemistry, Xinjiang University, Urumqi, Xinjiang, PR China

‡ Lihui Zhan and Jindou Hu with equal contributions to this work.

Corresponding Author

* E-mail: caoyali523@163.com (Y. Cao); h1061717965@163.com (A. Hao)

Experimental section

S1. Chemicals

The analytical grade raw materials used in the synthesis obtained from commercial sources without the need for further purification. Bismuth nitrate pentahydrate ($Bi(NO_3)_3·5H_2O$, AR, 99.0%, Chengdu Cologne Chemical Co.), potassium chloride (KBr, AR, 99.0%, Tianjin Zhiyuan Chemical Reagent Co.), Cerium(IV) sulfate tetrahydrate ($Ce(SO_4)_2·4H_2O$, AR, 99.0%, Aladdin), methanol (CH_3OH, AR, 99.5%, Tianjin Yongsheng Fine Chemical Reagent), ethanol (CH_3CH_2OH, AR, 75%, Tianjin Yongsheng Fine Chemical Reagent).

S2. Synthesis of BiOBr and Ce–doped BiOBr piezocatalysts

The BiOBr piezocatalyst was synthesized using a facile one–step hydrothermal method. In detail, 3 mmol of $Bi(NO_3)_3·5H_2O$ was added to 30 mL of deionized water and subjected to sonication and dispersion for 30 min. The resulting well–dispersed solution was named A. Additionally, 3 mmol of KBr was added to 30 mL of deionized water and stirred for 30 min for dispersion, respectively. This well–dispersed solution was named B. Next, solution B was added to solution A and mixed well, continuing stirring for 30 min. Then, the suspension obtained from the previous step was transferred to a 100 mL Teflon–lined stainless steel autoclave and heated hydrothermally at 160 °C for 6 h. After completion of the hydrothermal treatment, the autoclave was allowed to cool naturally to room temperature. Finally, the piezocatalyst was washed thrice with water and ethyl alcohol, and dried at 60 °C for 12 h in ambient air.

The Ce–doped BiOBr piezocatalysts were synthesized using a facile one–step hydrothermal method. In detail, 3 mmol of $Bi(NO_3)_3·5H_2O$ was added into 30 mL of deionized water and subjected to sonication and dispersion for 30 min. The resulting well–dispersed solution was named A. Additionally, 3 mmol of KBr and different amount (0.03, 0.15 and 0.30 mmol) of $Ce(SO_4)_2·4H_2O$ were added to 30 mL of deionized water and stirred for 30 min for dispersion, respectively. This well–dispersed solution was named B. Next, solution B was added to solution A and mixed well, continuing stirring for 30 min. Then, the suspension obtained from the previous step was transferred to a 100 mL Teflon–lined stainless steel autoclave and heated hydrothermally at 160 °C for 6 h. After completion of the hydrothermal treatment, the autoclave was allowed to cool naturally to room temperature. Finally, the piezocatalysts were washed thrice with water and

ethyl alcohol, and dried at 60 °C for 12 h in ambient air. The molar percentage of Ce elemental to Bi was controlled at various levels: 0.01, 0.05, and 0.1. Consequently, the corresponding obtained samples were denoted as 1% Ce–BiOBr, 5% Ce–BiOBr and 10% Ce–BiOBr. The synthesis procedures are depicted in Fig. S1.

S3. Characterization of Piezocatalysts

Crystal structures of BiOBr and Ce–BiOBr catalysts were analyzed using X–ray powder diffraction (XRD) techniques employing the Bruker D8 instrument. The surface chemical states of the samples were characterized through X–ray photoelectron spectroscopy (XPS) using the Thermo Fisher Scientific ESCALAB250Xi instrument. The presence of OVs in the catalyst was examined through electron paramagnetic resonance (EPR) spectroscopy using an A300 Bruker electron spin paramagnetic resonance meter. The morphology and components of the catalysts were examined using field emission scanning electronic microscopy (SEM) with the Hitachi S–4800 microscope equipped with an energy dispersive spectrometer (EDS), as well as transmission electron microscopy (TEM) and high–resolution transmission electron microscopy (HRTEM) utilizing the JEOL JEM–2100F microscope. The surface area and pore size distribution of the catalysts were investigated by the Brunauer–Emmett–Teller (BET) method with Autosorb–iQ. Ultraviolet–visible (UV–vis) absorption spectra were measured using the UV–2601 spectrophotometer. UV–vis diffuse reflectance spectra (DRS) were obtained using the U–3900H spectrophotometer from Hitachi. The presence of hydroxyl ($^{\bullet}OH$) and superoxide ($^{\bullet}O_2^-$) radicals were measured using an EPR spectrometer with MEX–nano, Bruker. The amount of H_2 produced was measured using a GC–9790, Fu Li, China gas chromatograph.

S4. Piezocatalytic Performances Measurements

S4.1. Piezocatalytic H_2 evolution Performances Measurements

First, 50 mg of piezocatalyst was added to separate borosilicate headspace flasks, along with 16 mL of deionized water and 4 mL of methanol (MeOH).[1,2] Subsequently, the vials were evacuated for 20 min and then passed through argon gas to completely remove the air. The gas mixture in the vials was tested at ultrasonic power to evaluate the piezocatalytic activity under offline conditions. To measure the amount of H_2 produced, a certain volume of the gas component was periodically collected from the reaction systems and injected into a GC–9790 gas

chromatograph, Fu Li, China. All experiments were repeated three times and the average value was taken as the data of piezocatalytic activity, with error bars representing the standard deviation of three repeated experiments.

S4.2. Piezocatalytic degradation organic pollutant performances measurements

The piezocatalytic efficacy of these catalysts was assessed by their ability to degrade organic pollutant, specifically methyl orange (MO), using an ultrasonic cleaner operating at a frequency of 40 kHz and a power of 150 W. Initially, 25 mg of the piezocatalyst was dispersed in a 50 mL solution of MO. This mixture was stirred in the dark for approximately 30 minutes to establish an adsorption–desorption equilibrium between the piezocatalyst and MO prior to ultrasonic treatment. Then about 3 mL of the suspension was sampled at fixed intervals and quickly centrifuged. Finally, the centrifuged solutions were measured by UV–vis absorption spectroscopy using a UV–2601 spectrophotometer. Each experiment was conducted three times, and the average value was recorded as the catalytic activity data, with error bands indicating the standard deviation.

In addition, various scavengers were employed to elucidate the roles of different reactive species in the degradation process. Silver nitrate ($AgNO_3$), ethylenediaminetetraacetic acid disodium salt (EDTA–2Na), benzoquinone (BQ) and isopropanol (IPA) scavengers were corresponded to the capture of e^-, h^+, $^{\bullet}O_2^-$ and $^{\bullet}OH$ radicals, respectively. Furthermore, the presence of $^{\bullet}OH$ and $^{\bullet}O_2^-$ radicals, generated through 5,5–dimethyl–1–pyrroline N–oxide (DMPO), were measured using an EPR spectrometer.

S5. Piezo–electrochemical performances measurements

To investigate the electrochemical properties, piezo–current measurements, electrochemical impedance spectroscopy (EIS) and Mott–Schottky (MS) patterns were conducted based on related reports.[3–5] These measurements were conducted on the electrochemical workstation (CHI 760E, Shanghai Chenhua) by a typical three–electrode system. During the measurement process, 5 mg of catalyst was dissolved in 80 μL of anhydrous ethanol for proper dispersion and then coated on the ITO glass for drying before testing. An Ag/AgCl electrode served as the reference electrode, while a Pt sheet served as the counter electrode. The 0.5 M of Na_2SO_4 aqueous solution was served as the electrolyte. Transient piezo–current response curves were conducted during the ultrasonic cycles and the time interval of ultrasonic vibration was 20 s. EIS Nyquist plots measurement were

performed in the frequency range from 0.1 to 10^5 Hz with an amplitude set at 5 mV. The Mott–Schottky curves were performed at an amplitude of 10 mV. Besides, the mechanical source was consistent with the ones in the piezocatalytic experiment.

Figures

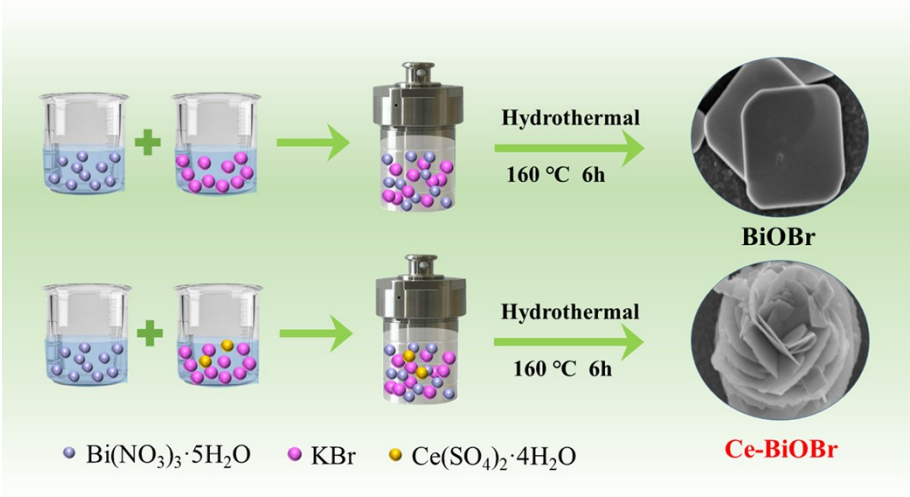

Fig. S1 Synthesis diagram of BiOBr and Ce–BiOBr catalysts

The thinner nanosheets of BiOBr are mainly attributed to the strong interaction from doping Ce atoms with Bi, affecting the stacking of $[Bi_2O_2]^{2+}$ and $[Br_2]^{2-}$ slabs by inhibiting the growth of crystal nuclei. With a further increase in Ce doping concentration (e.g. 5%, 10%), the nanosheets of BiOBr agglomerate to form nanoflower–like structures through a self–assembly approach.[6–8]

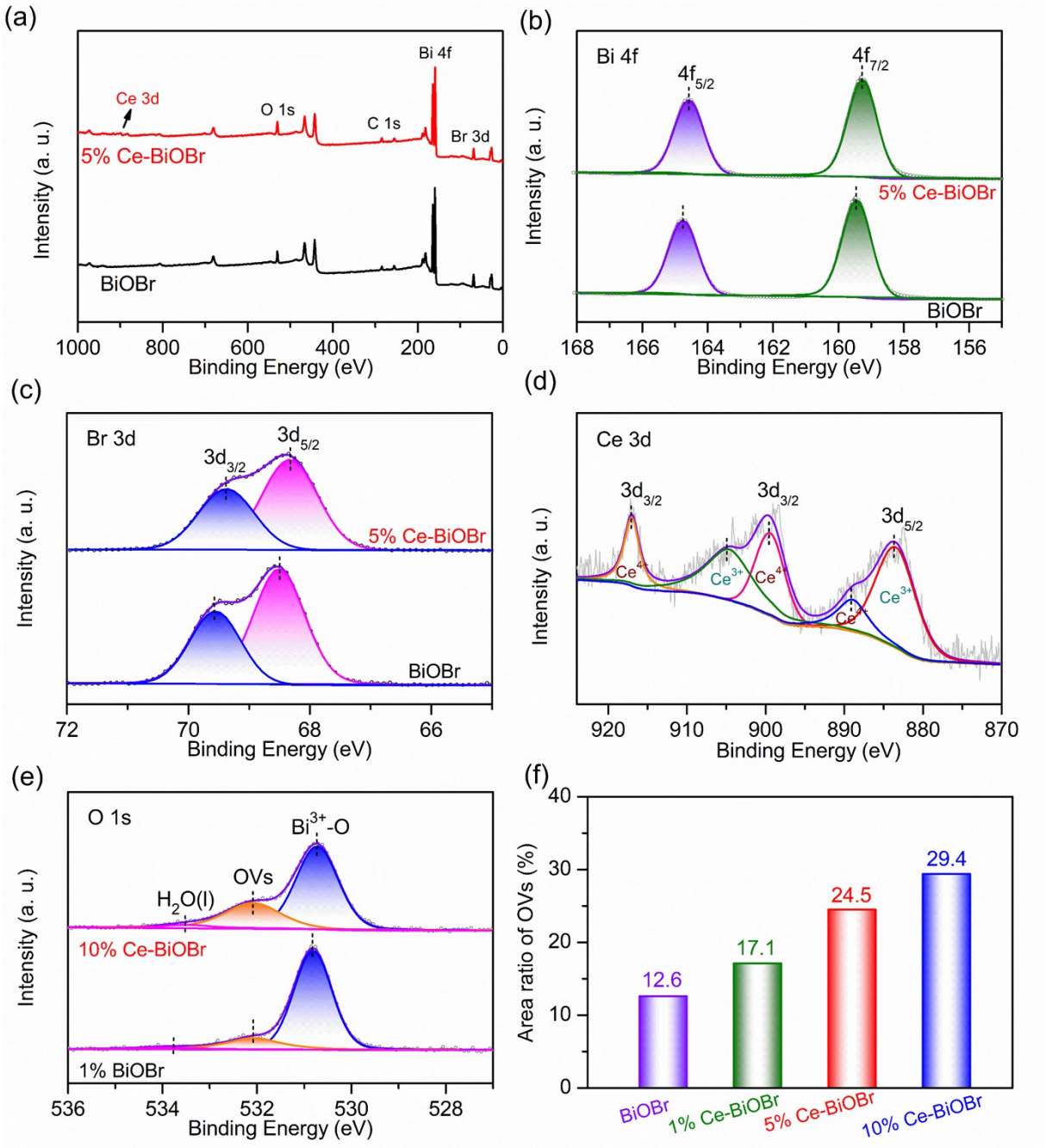

Fig. S2 (a) XPS survey spectra of BiOBr and 5% Ce–BiOBr. High–resolution XPS scan spectra of (b) Bi 4f and (c) Br 3d of BiOBr and 5% Ce–BiOBr. (d) Ce 3d of 5% Ce–BiOBr. (e) High–resolution XPS scan spectra of O1s for 1% Ce–BiOBr and 10% Ce–BiOBr. (f) The area ratio of OVs in BiOBr and (1%, 5%, 10%) Ce–BiOBr.

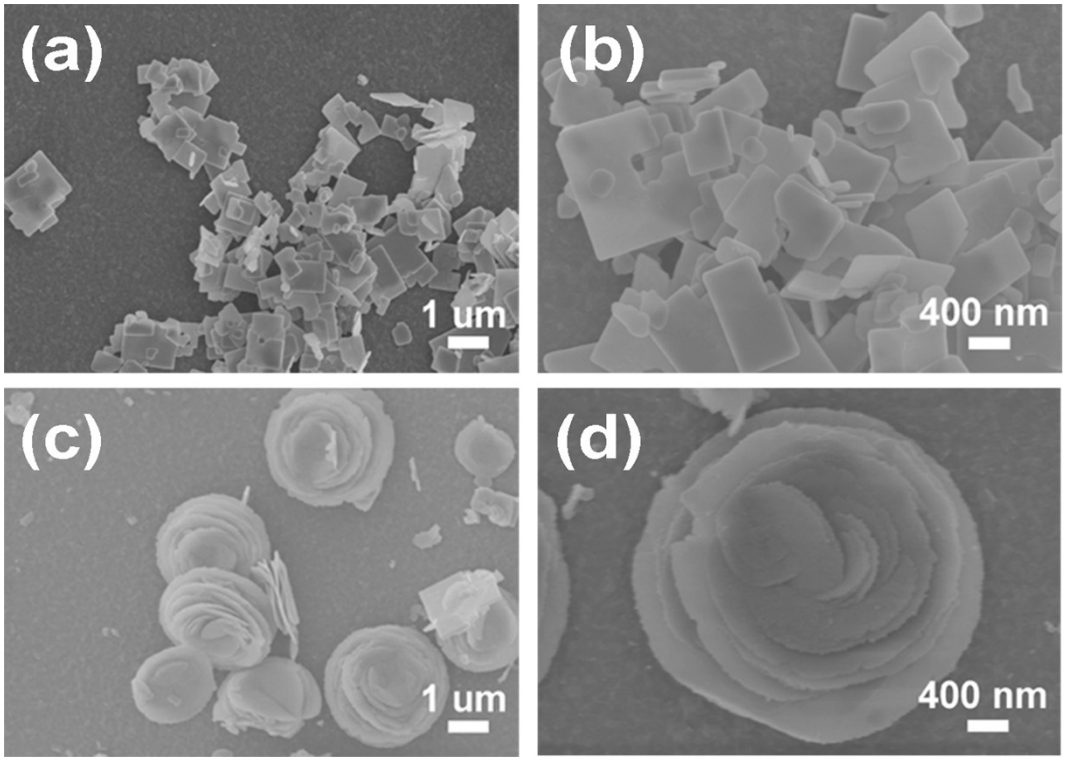

Fig. S3 SEM images of (a-b) 1% Ce–BiOBr and (c-d) 10% Ce–BiOBr.

As seen in Fig. S3 (a-b), the size of nanosheets in 1% Ce–BiOBr became smaller and thinner. As the Ce content continued to increase, the nanosheets stacked together to form a 3D flower–like structure with uniform size in 10% Ce–BiOBr as shown in Fig. S3 (c-d).

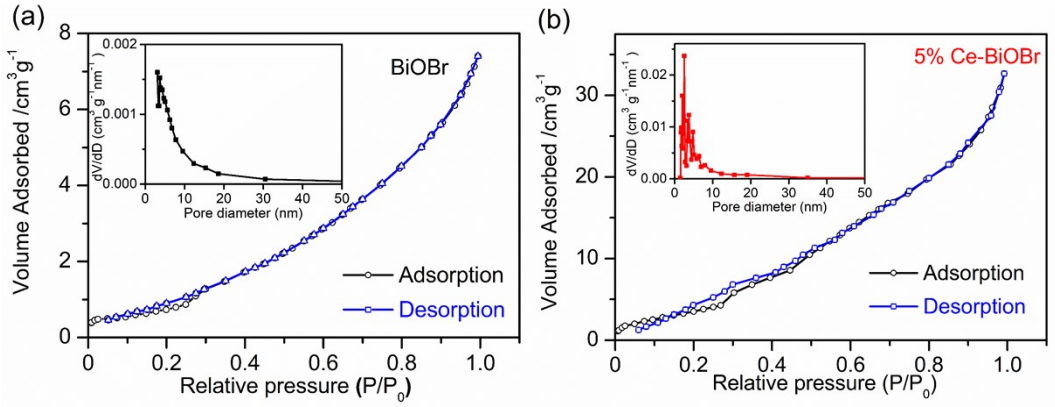

Fig. S4 (a) Typical N_2 adsorption–desorption isotherms of BiOBr, the inset shows the corresponding pore size distribution. (b) Typical N_2 adsorption–desorption isotherms of 5% Ce–BiOBr, the inset shows the corresponding pore size distribution.

Flower–like structure materials often have large specific surface area, and the abundant active sites could promote the piezocatalytic activity. Therefore, N_2 adsorption–desorption isotherms of BiOBr and 5% Ce–BiOBr were tested as shown in Fig. S4. The measured results

show that the specific surface area of 5% Ce–BiOBr is 46.7 $m^2 g^{-1}$, more than seven times that of BiOBr (6.1 $m^2 g^{-1}$). The insets of Fig. S4 (a-b) also show the pore size distributions of BiOBr and 5% Ce–BiOBr, respectively. These results suggest that 5% BiOBr has a larger specific surface area, higher pore volume and volumetric adsorption capacity in Table S2, which is beneficial for improving piezocatalytic activity, to a certain extent.[9,10]

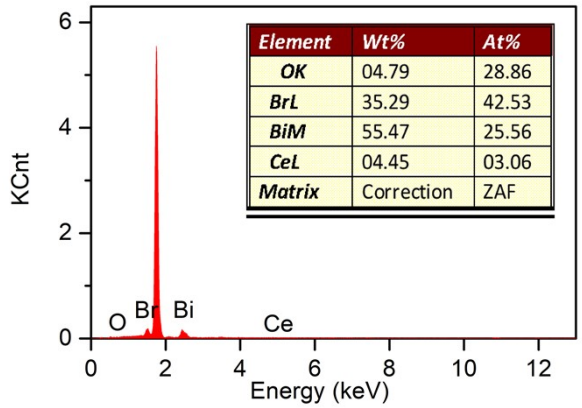

Fig. S5 EDS energy spectrum of 5% Ce–BiOBr.

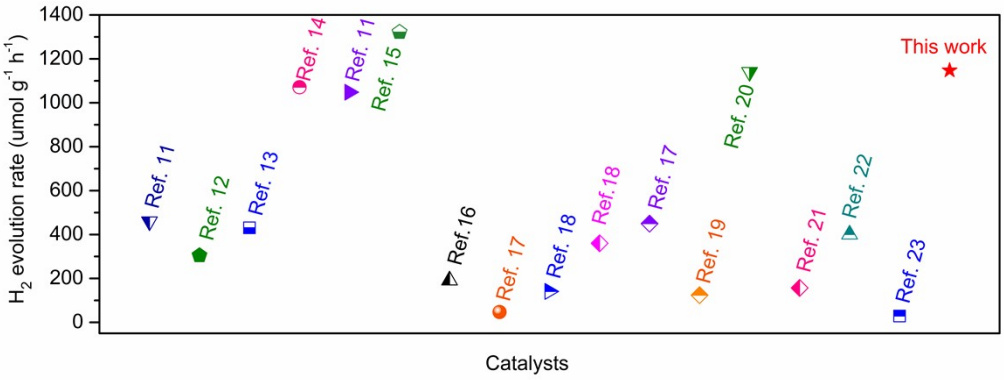

Fig. S6 Comparison of H_2 evolution performance of 5% Ce–BiOBr with others reported piezocatalysts.

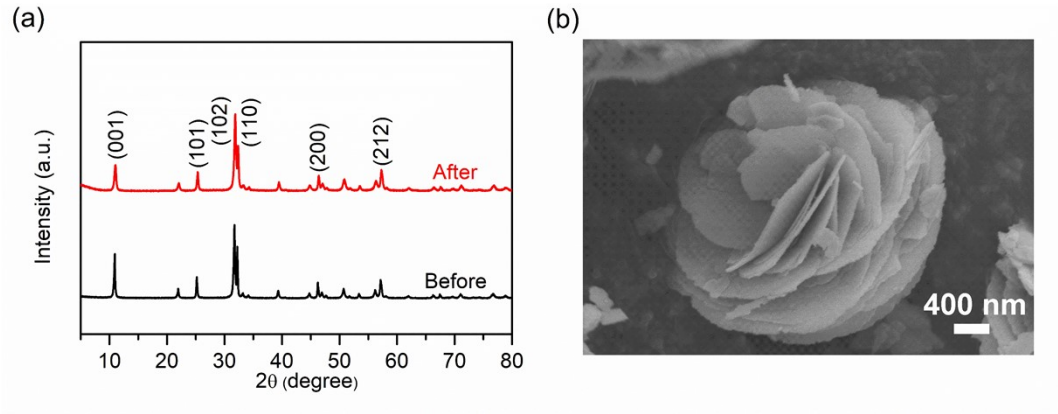

Fig. S7 (a) XRD patterns and (b) SEM image of 5% Ce–BiOBr at after the stability test for piezocatalytic H_2 evolution.

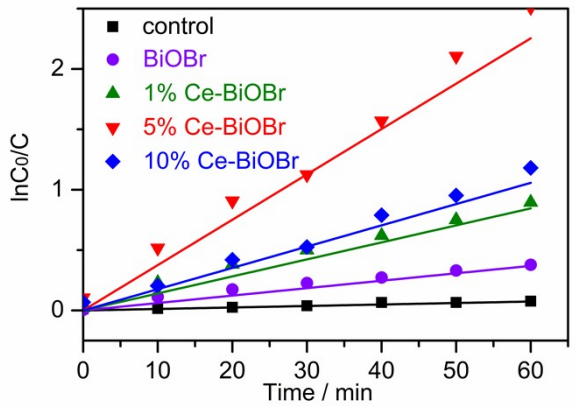

Fig. S8 The plot of $\ln(C_0/C)$–t for piezocatalytic degradation.

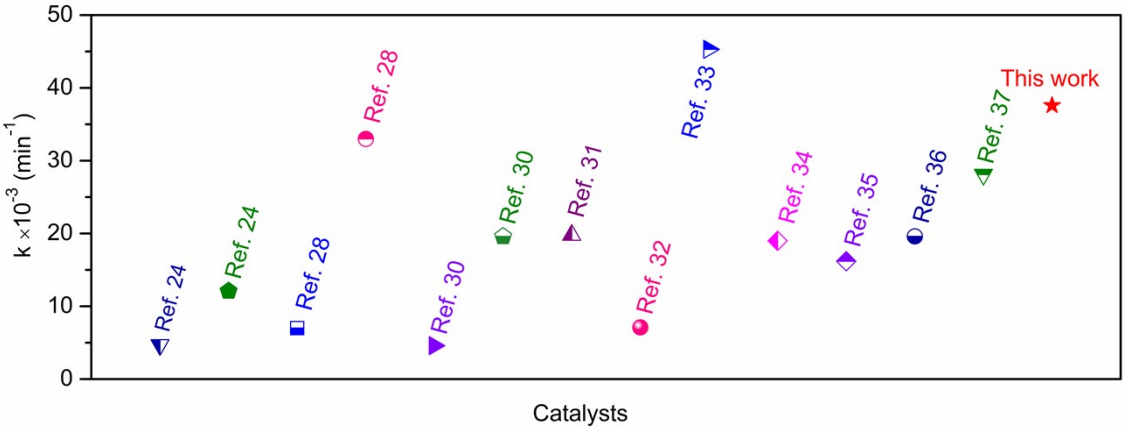

Fig. S9 Comparison of reaction kinetics constant of k in 5% Ce–BiOBr with other reported piezocatalysts.

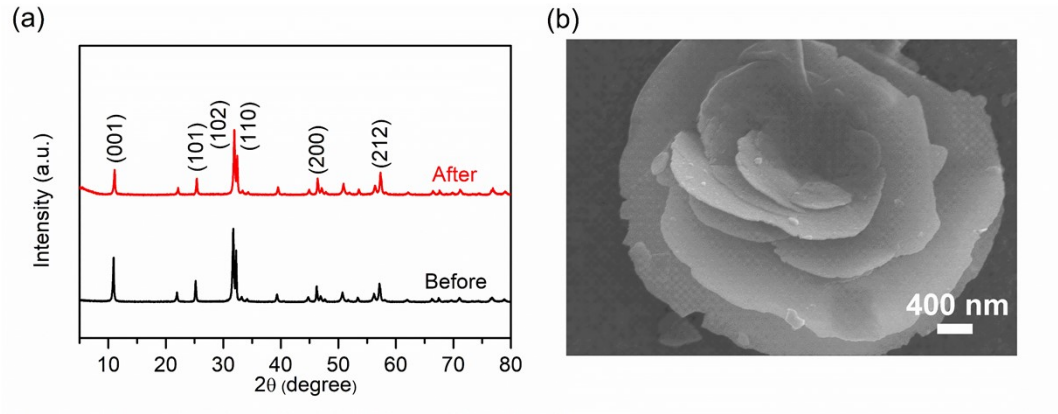

Fig. S10 (a) XRD patterns and (b) SEM image of 5% Ce–BiOBr at after the stability test for piezocatalytic degradation of MO.

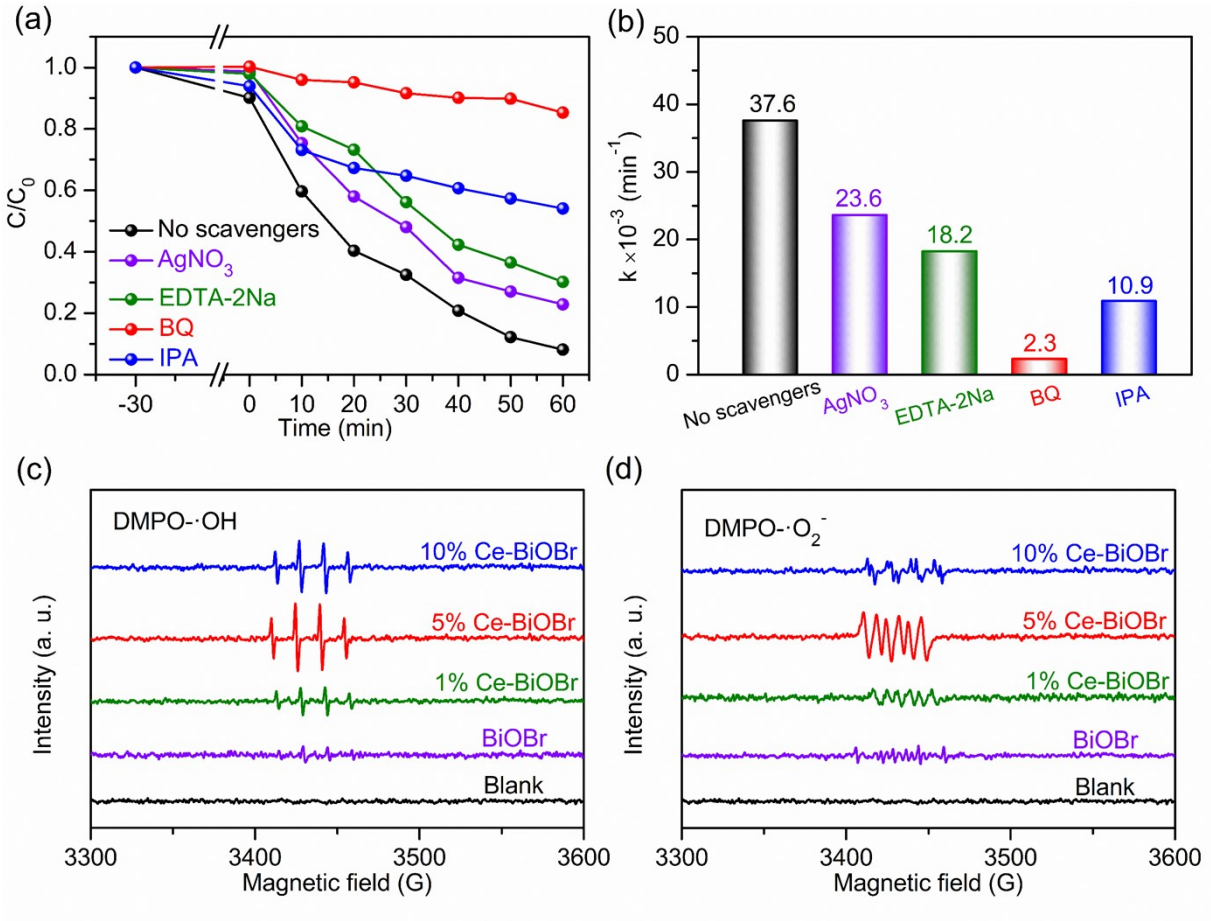

Fig. S11 (a) Radical scavenging experiments and (b) corresponding reaction kinetics constant k of 5% Ce–BiOBr for piezocatalytic degradation MO dye process. EPR spectra of (c) DMPO–•OH and (d) DMPO–•O_2^- of blank, BiOBr and (1%, 5% and 10%) Ce–BiOBr.

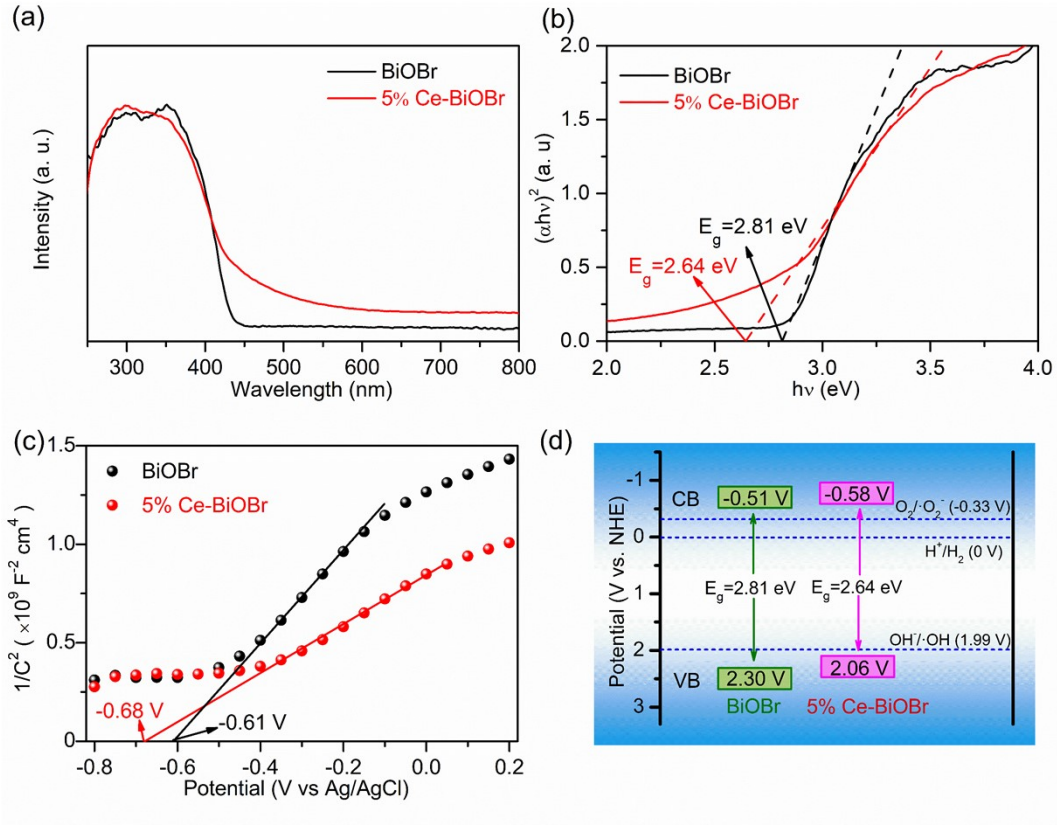

Fig. S12 (a) UV–vis diffuse reflectance spectra. (b) Calculated band gap, (c) Mott–Schottky plots and (d) Energy band structure diagram of BiOBr and 5% Ce–BiOBr.

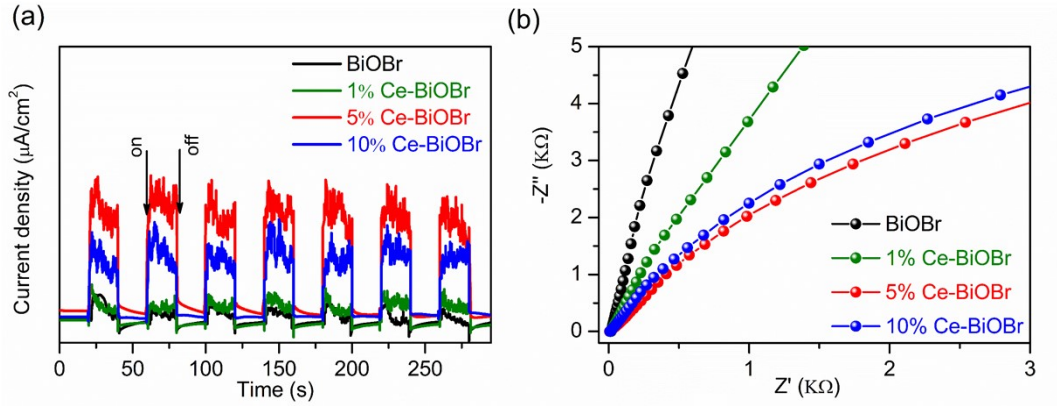

Fig. S13 (a) Transient current responses and (b) EIS Nyquist plots of BiOBr and (1%, 5% and 10%) Ce–BiOBr, respectively.

Table S1. The area ratio of various O species in BiOBr and Ce–BiOBr.

Samples	O_L (%)	O_V (%)	O_A (%)
BiOBr	83.0	12.6	4.4
1% Ce–BiOBr	79.5	17.1	3.4
5% Ce–BiOBr	72.9	24.5	2.6
10% Ce–BiOBr	68.6	29.4	2.0

Table S2. Surface property of BiOBr and 5% Ce–BiOBr.

Sample	Specific surface ($m^2\ g^{-1}$)	Pore volume ($cm^3\ g^{-1}$)	Aperture (nm)
BiOBr	6.1	0.01	3.06
5% Ce–BiOBr	46.7	0.06	2.53

Table S3. The elemental contents of 5% Ce–BiOBr by EDS.

Element	Wt%	At%
O	4.79	28.86
Br	35.29	42.53
Bi	55.47	25.56
Ce	4.45	3.06

Table S4. Comparison of H_2 evolution performance over catalysts previously reported with this work.

Piezocatalysts	Sacrificial Agents	Conditions	H_2 evolution rates ($\mu mol\ g^{-1}\ h^{-1}$)	Ref.
BiOCl	Methanol	120 W, 40 kHz	459.7	[11]
$BaTiO_3$	Methanol	180 W, 35 kHz	305.0	[12]
$SrTiO_3$	Methanol	300W, 40 kHz	430.8	[13]
$MoSe_2$	Methanol	300 W, 59 kHz	1071.0	[14]
CdS/BiOCl	Methanol	120 W, 40 kHz	1048.2	[11]
$0.7BiFeO_3/0.3BaTiO_3$	Methanol	100 W, 40 kHz	1322.0	[15]
Bi_2WO_6	Triethanolamine	40 kHz	191.3	[16]
$(Na_{0.5}Bi_{0.5})TiO_3$–$Ba(Ti_{0.5}Ni_{0.5})O_3$	Triethanolamine	200 W, 40 kHz	47.4	[17]
$BaTi_{0.89}Sn_{0.11}O_3$	Triethanolamine	120 W, 40 kHz	141.1	[18]
Ag–$BaTi_{0.89}Sn_{0.11}O_3$	Triethanolamine	120 W, 40 kHz	360.2	[18]
$(Na_{0.5}Bi_{0.5})TiO_3$–Ba$(Ti_{0.5}Ni_{0.5})O_3$/Ag	Triethanolamine	200 W, 40 kHz	450.0	[17]
$BiFeO_3$	Na_2SO_3	100 W, 45 kHz	124.1	[19]
$BiFeO_3$/Pd	Na_2SO_3	100 W, 40 kHz	1140	[20]
CdS	Na_2SO_3	150 W, 40 kHz	157.0	[21]
$PbTiO_3$/CdS	Na_2S/Na_2SO_3	40 kHz	400.6	[22]
MoS_2	$FeSO_4$	110 W, 40 kHz	29.1	[23]
BiOBr	Methanol	150 W, 40 kHz	601.1	This work
5% Ce–BiOBr	Methanol	150 W, 40 kHz	1147.6	This work

Table S5. Comparison piezocatalytic degradation of organic pollutants performances over catalysts previously reported with this work.

Piezocatalysts	**Dyes species and concentration**	**Conditions**	**Rate constant (min^{-1})**	**Reference**
BiOBr	MO, 10 mg/L	120 W, 40 kHz	0.0047	[24]
$BiOBr/BaTiO_3$	MO, 10 mg/L	120 W, 40 kHz	0.0121	[24]
BiOBr	RhB, 10 mg/L	120 W, 40 kHz	0.0067	[25]
BiOBr	TC, 10 mg/L	60 W, 40 kHz	0.0056	[26]
AuPt/BiOBr	TC, 10 mg/L	60 W, 40 kHz	0.0127	[26]
BiOBr	MV, 20 mg/L	/	0.0057	[27]
$Bi_2MoO_6/BiOBr$	MV, 20 mg/L	/	0.0098	[27]
Bi_5O_7I	MO, 10 mg/L	60 W, 40 kHz	0.0070	[28]
Ag/Bi_5O_7I	MO, 10 mg/L	60 W, 40 kHz	0.0330	[28]
Au–BiOBr	CBZ, 5 mg/L	120 W, 40 kHz	0.0052	[29]
ZnO	MO, 10 mg/L	150 W, 40 kHz	0.0046	[30]
Ag–ZnO	MO, 10 mg/L	150 W, 40 kHz	0.0196	[30]
$0.93(Ba_{1/2}Na_{1/2})TiO_3–0.07BaTiO_3$	MO, 10 mg/L	100 W, 40 kHz	0.0198	[31]
$(Ba_{0.85}Ca_{0.15})(Ti_{0.9}Zr_{0.1})O_3$	MO, 5 mg/L	120 W, 40 kHz	0.0071	[32]
Sm–PMN–0.29PT	MO, 5 mg/L	40 kHz	0.0453	[33]
$BaTiO_3$–1200	MO, 5 mg/L	80 W, 40 kHz	0.0190	[34]
$Ag–BaTiO_3$	MO, 5 mg/L	120 W, 40 kHz	0.0162	[35]
$(Ba,Sr)TiO_3$	MO, 5 mg/L	80 W, 40 kHz	0.0196	[36]
$Ba_{0.8}Sr_{0.2}TiO_3$	MO, 5 mg/L	120 W, 40 kHz	0.0281	[37]
BiOBr	MO, 5 mg/L	150 W, 40 kHz	0.0062	This work
5% Ce–BiOBr	MO, 5 mg/L	150 W, 40 kHz	0.0376	This work

References

1. Z. Wang, T. Hu, H. He, Y. Fu, X. Zhang, J. Sun, L. Xing, B. Liu, Y. Zhang and X. Xue, *ACS Sustain. Chem. Eng.*, 2018, **6**, 10162–10172.
2. X. Xiong, Y. Wang, J. Ma, Y. He, J. Huang, Y. Feng, C. Ban, L.–Y. Gan and X. Zhou, *Appl. Surf. Sci.*, 2023, **616**.
3. D. Yu, Z. Liu, J. Zhang, S. Li, Z. Zhao, L. Zhu, W. Liu, Y. Lin, H. Liu and Z. Zhang, *Nano Energy*, 2019, **58**, 695–705.
4. L. Tan, X. Sun, J. Zhang, C. Jin, F. Wang and D. Liu, *Dalton Trans.*, 2023, **52**,14210.
5. J. Ma, J. Ren, Y. Jia, Z. Wu, L. Chen, N. O. Haugen, H. Huang and Y. Liu, *Nano Energy*, 2019, **62**, 376–383.
6. Y. Jin, Fan Li, T. Li, X. Xing, W. Fan, L. Zhang and C. Hu, *Appl. Catal., B*, 2022, **302**, 120824.
7. J. Wu, Y. Xie, Y. Ling, J. Si, X. Li, J. Wang, Hao. Ye, J. Zhao, S. Li, Q. Zhao and Y. Hou, *Chem. Eng. J*, 2020, **400**, 125944.
8. J. Hao, Y. Zhang, L. Zhang, J. Shen, L. Meng and X. Wang, *Chem. Eng. J*, 2023, **464**, 142536.
9. Y. Jin, J. Zhang, S. Wang, X. Wang, M. Fang, Q. Zuo, M. Kong, Z. Liu and X. Tan, *J. Environ. Chem. Eng.*, 2022, **10**, 107675.
10. P. Wang, X. Li, S. Fan, X. Chen, M. Qin, D. Long, M.O. Tadé, S. Liu, *Appl. Catal. B*, 2020, **279**, 119340.
11. P. Hao, Y. Cao, X. Ning, R. Chen, J. Xie, J. Hu, Z. Lu and A. Hao, *J. Colloid Interface Sci.*, 2023, **639**, 343–354.
12. Q. Tang, J. Wu, D. Kim, C. Franco, A. Terzopoulou, A. Veciana, J. Puigmartí-Luis, X. Z. Chen, B. J. Nelson and S. Pané, *Adv. Funct. Mater.*, 2022, **32**, 2202180.
13. Y. Jiang, J. Xie, Z. Lu, J. Hu, A. Hao and Y. Cao, *J. Colloid Interface Sci.*, 2022, **612**, 111–120.
14. Y. J. Chung, C. S. Yang, J. T. Lee, G. H. Wu and J. M. Wu, *Adv. Enerdy. Mater.*, 2020, **10**, 2002082.
15. Y. Sun, X. Li, A. Vijayakumar, H. Liu, C. Wang, S. Zhang, Z. Fu, Y. Lu and Z. Cheng, *ACS Appl. Mater. Interfaces*, 2021, **13**, 11050–11057.

16. X. Xu, L. Xiao, Z. Wu, Y. Jia, X. Ye, F. Wang, B. Yuan, Y. Yu, H. Huang and G. Zou, *Nano Energy*, 2020, **78**, 105351.
17. H. Xiao, W. Dong, Q. Zhao, F. Wang and Y. Guo, *J. Hazard. Mater.*, 2021, **416**, 125808.
18. Q. Zhao, H. Xiao, G. Huangfu, Z. Zheng, J. Wang, F. Wang and Y. Guo, *Nano Energy*, 2021, **85**, 106028.
19. H. You, Z. Wu, L. Zhang, Y. Ying, Y. Liu, L. Fei, X. Chen, Y. Jia, Y. Wang, F. Wang, S. Ju, J. Qiao, C. H. Lam and H. Huang, *Angew. Chem. Int. Ed.*, 2019, **58**, 11779–11784.
20. G. Yang, Q. Chen, W. Wang, S. Wu, B. Gao, Y. Xu, Z. Chen, S. Zhong, J. Chen and S. Bai, *ACS Appl. Mater. Interfaces*, 2021, **13**, 15305–15314.
21. J. Wang, C. Hu, Y. Zhang and H. Huang, *Chin. J. Catal*., 2022, **43**, 1277–1285.
22. X. Huang, R. Lei, J. Yuan, F. Gao, C. Jiang, W. Feng, J. Zhuang and P. Liu, *Appl. Catal. B*, 2021, **282**, 119586.
23. S. Li, Z. Zhao, D. Yu, J.–Z. Zhao, Y. Su, Y. Liu, Y. Lin, W. Liu, H. Xu and Z. Zhang, *Nano Energy*, 2019, **66**, 104083.
24. X. Zhou, F. Yan, S. Wu, B. Shen, H. Zeng and J. Zhai, *Small*, 2020, **16**, 2001573.
25. H. Lei, H. Zhang, Y. Zou, X. Dong, Y. Jia and F. Wang, *J. Alloys Compd.*, 2019, **809**, 151840
26. T. Xian, X. Sun, L. Di, C. Sun, H. Li, C. Ma and H. Yang, *Appl. Surf. Sci.*, 2023, **638**, 158136.
27. Z. Yao, H. Sun, S. Xiao, Y. Hu, X. Liu and Y. Zhang, *Appl. Surf. Sci.*, 2021, **560**, 150037.
28. L. Chen, W. Zhang, J. Wang, X. Li, Y. Li, X. Hu, L. Zhao, Y. Wu and Y. He, *Green. Energy. Environ.*, 2023, **8**, 283–295.
29. J. Hu, Y. Chen, Y. Zhou, L. Zeng, Y. Huang, S. Lan and M. Zhu, *Appl. Catal. B*, 2022, **311**, 121369.
30. X. Ning, A. Hao, Y. Cao, N. lv and D. Jia, *Appl. Surf. Sci.*, 2021, **566**, 150730.
31. D. Liu, Y. Song, Z. Xin, G. Liu, C. Jin and F. Shan, *Nano Energy*, 2019, **65**, 104024.
32. C. C. Jin, C. H. Liu, X. C. Liu, Y. Wang and H. L. Hwang, *Ceram. Int.*, 2018, **44**, 17391–17398.
33. B. Yuan, J. Wu, N. Qin, E. Lin, Z. Kang and D. Bao, *Appl. Mater. Today.*, 2019, **17**, 183–192.
34. J. Wu, Q. Xu, E. Lin, B. Yuan, N. Qin, S. K. Thatikonda and D. Bao, *ACS Appl. Mater. Interfaces*, 2018, **10**, 17842–17849.

35. E. Lin, J. Wu, N. Qin, B. Yuan and D. Bao, *Catal. Sci. Technol.*, 2018, **8**, 4788–4796.
36. B. Yuan, J. Wu, N. Qin, E. Lin and D. Bao, *ACS Appl. Nano. Mater.*, 2018, **1**, 5119–5127.
37. J. Wu, N. Qin, E. Z. Lin, Z. H. Kang and D. H. Bao, *Mater. Today. Energy.*, 2021, **21**, 100732.